Arch. Mech., **58**, 3, pp. 273–291, Warszawa 2006

Experimental and theoretical investigations of glass-fibre reinforced composite subjected to uniaxial compression for a wide spectrum of strain rates

E. A. PIECZYSKA[1)], R. B. PĘCHERSKI[1)], S. P. GADAJ[1)], W. K. NOWACKI[1)], Z. NOWAK[1)], M. MATYJEWSKI[2)]

[1)] *Institute of Fundamental Technological Research*
Polish Academy of Sciences
Świętokrzyska 21, 00-049 Warsaw, Poland

[2)] *Warsaw University of Technology*

Results of static and dynamic compression tests for two types of glass fibre-reinforced polypropylene composites are presented. Stress-strain curves showing the influence of the strain rate on the composite mechanical properties have been obtained. A three-dimensional description of the material behavior during the deformation has been developed. The material constitutive parameters have been calculated. Specification of the parameters and description of the methods used for their identification have been worked out. The results are discussed in terms of the deformation processes and the material non-homogeneity.

1. Introduction

The behaviour of composites at quasistatic and dynamic rates of deformation has been of considerable interest during recent years. Composites represent an important class of materials, which have now become indispensable in car, aircraft and other industries. Their mechanical characteristics over a wide range of strain rates are very important, as they are often applied as energy absorbers, i.e. subjected to impact. Particularly attractive are the tests in compression and shear, because machine parts often work in such deformation modes.

Studies of the behaviour of composite materials at high strain rates have been performed for many years but reliable data on strain-rate effects is very scarce. Tay *et al.* [1] presented an empirical strain rate-dependent constitutive relationship for glass-fibre reinforced epoxy and pure epoxy. The range of strain rates used was between 5×10^{-4} s^{-1} and 2.5×10^{3} s^{-1}. A comparison between the behaviour of pure epoxy and reinforced epoxy revealed that both are strain rate-sensitive, especially in the low strain rate regime. An empiri-

cal equation incorporating both strain and strain rate terms was proposed and was found to adequately describe the stress-strain behaviour of both materials. Horst *et al.* [2] investigated the fibre-matrix debonding stress for short fibre-reinforced materials with matrix plasticity. Finite element modelling was applied and experimental verification performed. Fitoussi *et al.* [3] developed a statistical model that correlates the microstructure and its local perturbations, to the macroscopic behaviour. The objective of their paper was to predict the entire stress/strain curves and the loss of stiffness with damage for sheet-molding-compound (SMC) composites. In the case of an SMC composite with 32% fibre volume fraction, debonding at the fibre/matrix interfaces was the predominant damage mechanism. In their paper, a relationship between the statistics of interface failure and the scatter observed in the macroscopic mechanical test results was demonstrated.

The flow of the material during the molding process results in different degrees of fiber alignment and as a consequence in material anisotropy. The problem of fiber alignment in an SMC and its influence on the material strength was studied by Pinfold *et al.* [4]. They compared experimental and numerical results. Camanho and Matthews [5] developed a three-dimensional finite element model with a three-dimensional failure criterion and a constitutive equation that takes into account the effects of damage on the material elastic properties. Piry and Michaeli [6] presented a stiffness and failure analysis of SMC components, which takes into account anisotropic material properties. They found that SMC due to its material composition, i.e. polyester resin, chopped glass fibres and filler, represents a very heterogeneous material. The change from linear to nonlinear material behaviour is related to the occurrence of the first crack initiation in the matrix. In their model, fiber orientation distribution has been taken into account. Material properties measured under tensile loading showed a good correspondence with model results. An example of the strain-rate dependent model for metal matrix composites was presented by Ellyin and Xia [7].

The aim of our study is to combine experimental and theoretical investigations of the compression of a glass fibre-reinforced polypropylene composite subjected to loading over a wide spectrum of strain rates within the intermediate temperature range. By combination of the hydraulic servo-controlled universal machine and the technique of the Split Hopkinson Pressure Bar, it is possible to find the stress evolution versus plastic strain in so wide spectrum of the strain rates applied. A new approach is proposed, in which the mechanism of micro-shear banding in modelling of viscoplastic behaviour of the material is taken into account. The comprehensive experimental data obtained in quasistatic and dynamic tests made a basis for the identification of the proposed constitutive

model. The material considered belongs to the class of composites having an injection-moulded thermoplastic matrix containing chopped glass fibres. The glass transition temperature for polypropylene is 253 K. The flow pattern in injection moulding helps to align the fibres, so that proper mould design can give a stiff, strong product. This leads to inhomogeneous distribution of fibres and induced anisotropy of the mechanical properties. In the first modelling approach, homogeneity as well as isotropy of elastic and viscoplastic properties was assumed. However, the preliminary results of the experimental investigations revealed a certain anisotropy, which could be classified as orthotropic or transversal.

2. Compression test; experimental procedure

Investigations of compression were performed on disc specimens, cut off from polypropylene sheet composites denoted GB30 and GB40. The difference between them consisted in higher or lower glass-fiber volume contribution: 30% in the case of GB30 and 40% in the case of GB40. The diameter of the specimens was 12 mm and the thickness for the quasi-static compression tests was approximately 3 mm, equal to the composite sheet thickness. In order to minimize the inertia effects in the radial direction, occurring during dynamic investigations, the ratio of the thickness to the diameter of the specimen should be about 0.5 [8]. To satisfy this condition it was necessary to bond two cylindrical flat specimens, cut from the same composite sheet, with a very thin layer of cyanoacryl glue. As a result, specimens with a thickness of about 5.6 mm were obtained. The quasistatic compression tests were carried out in a hydraulic testing machine with the rates of deformation equal to 10^{-3} s^{-1}, 10^{-1} s^{-1}, 10^{1} s^{-1}.

In order to complete the set of results by inclusion of a higher rate of deformation, a modified Split Hopkinson Pressure Bar (SHPB) was used which enables obtaining the strain rate $\dot{\epsilon}$ value up to 10^{3} s^{-1}. Both quasi-static and dynamic tests were performed at room temperature 295 K. The surface of each specimen was covered with thin layer of anti-friction coating MoS_2 before the testing. Three tests were performed for each group of specimens to assure sufficient reliability of the results. The principle of the standard SHPB apparatus in terms of compression test is shown in Fig. 1.

The specimen S was placed between two bars made of high-strength steel. The incident B_i and the transmitter B_t bars have got the same length (1000 mm) and the same diameter (20 mm), which assures the same mechanical impedance. Three projectiles P (short, medium and long) were used in order to achieve various energies and related to this, various strain rates during the dynamic tests.

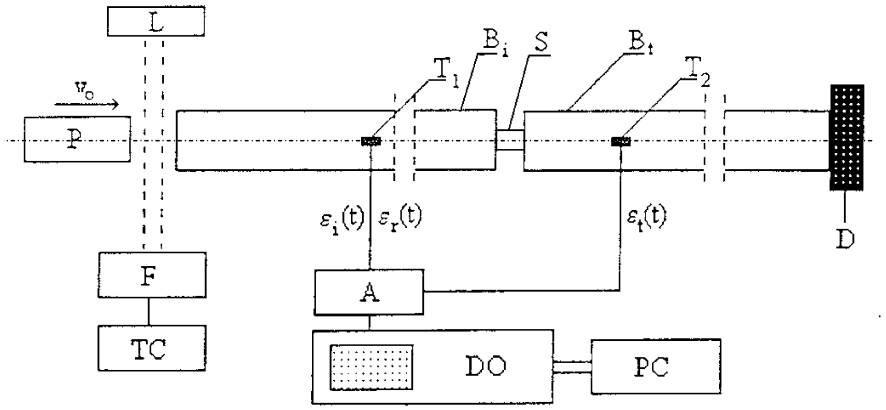

FIG. 1 Standard SHPB apparatus; P – projectile, B_i – incident bar, B_t – transmitter bar, S – specimen, D – damper, L – source of light, F – photodiodes, TC – time counter, T_1, T_2 – strain gauges, A – amplifier, DO – digital oscilloscope, PC – microcomputer.

2.1. Foundation of dynamic compression tests

The basic assumptions of the SHPB are well-known for many decades and are well documented [8, 9, 10].

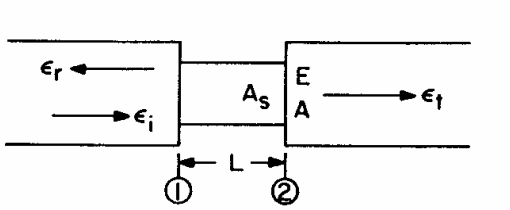

FIG. 2. Scheme of the specimen and strain pulses [9].

During dynamic compression, a thin cylindrical specimen is placed between two measuring bars (Fig. 2). If we take into account only the first passage of the wave along the bars, we can determine the change of the specimen thickness $\Delta l(t)$, the average strain ϵ, the average strain rate $\dot{\epsilon}$ and the average stress σ [10]:

$$\Delta l(t) = \delta_1(t) - \delta_2(t), \tag{2.1}$$

where δ_1 and δ_2 indicate displacements of the specimen ends (Fig. 2),

$$\epsilon(t) = \frac{c_0}{l_0} \int_0^t \Big[\varepsilon_i(\tau) - \varepsilon_r(\tau) - \varepsilon_t(\tau)\Big] d\tau, \tag{2.2}$$

$$\dot{\epsilon}(t) = \frac{c_0}{l_0} \Big[\epsilon_i(t) - \epsilon_r(t) - \epsilon_t(t)\Big], \tag{2.3}$$

$$\sigma(t) = \frac{E_0 A}{2A_s}\Big[\epsilon_i(t) + \epsilon_r(t) + \epsilon_t(t)\Big], \tag{2.4}$$

where: c_0 is the elastic-wave velocity in the Hopkinson bars, A – cross-section area of the bars, E_0 – Young's modulus of the bars, L_0– length of the specimen, A_s – cross-section area of the specimen.

If it is assumed that the forces at the ends of the specimen are equal to each other, then

$$\epsilon_i(t) = \epsilon_t(t) - \epsilon_r(t). \tag{2.5}$$

Making use of Eq. (2.5) in Eqs. (2.2)–(2.4), we obtain the stress, strain and strain rate, produced in the specimen:

$$\epsilon(t) = -\frac{2c_0}{l_0}\int_0^t \varepsilon_r(\tau)d\tau, \tag{2.6}$$

$$\sigma(t) = \frac{AE_0}{A_s}\epsilon_t(t), \tag{2.7}$$

$$\dot{\epsilon}(t) = -\frac{2c_0}{l_0}\epsilon_r(t). \tag{2.8}$$

These equations are used in order to calculate the mechanical characteristics of dynamic compression tests of the composite, where ϵ_i, ϵ_r and ϵ_t pulses were obtained from the test. It is important to note that the stress, the strain and the strain rate are average values, and that they were calculated under assumption of the uniaxial stress-state.

3. Experimental results

3.1. Quasistatic rates of deformation

The stress-strain relations obtained during uniaxial quasistatic compression of the composites studied are presented in Figs. 3, 4, 5. The curve's number in these pictures indicates the test number, GB30 or GB40 – the brand name of the composite. The stress and the strain quantities are referred to the current (instantaneous) value of the specimen cross-section and thickness values. An example of the stress-strain curves obtained during axial compression of 3 specimens of GB30 composite subjected to loading with the same strain rate is shown in Fig. 3. In the initial, elastic range of deformation, as well as during the unloading, a good repeatability of the obtained results is observed. However,

at higher strain some discrepancies between these curves were registered. This indicates a non-uniform distribution of the reinforcing composite fibers density, as well as their possible fracture.

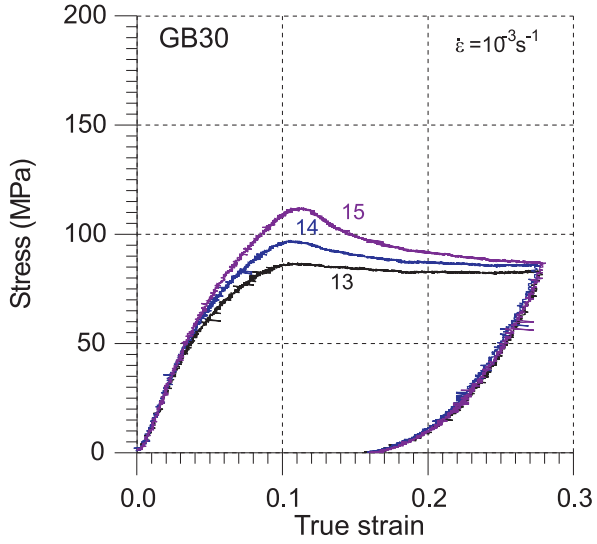

FIG. 3. Stress-strain relations of composite GB30 subjected to uniaxial compression test with strain rate $10^{-3}s^{-1}$.

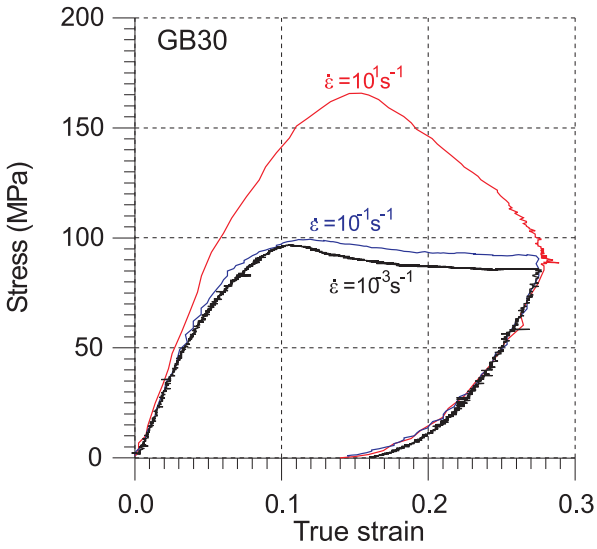

FIG. 4. Stress-strain relations of composite GB30 subjected to uniaxial compression test with various strain rates.

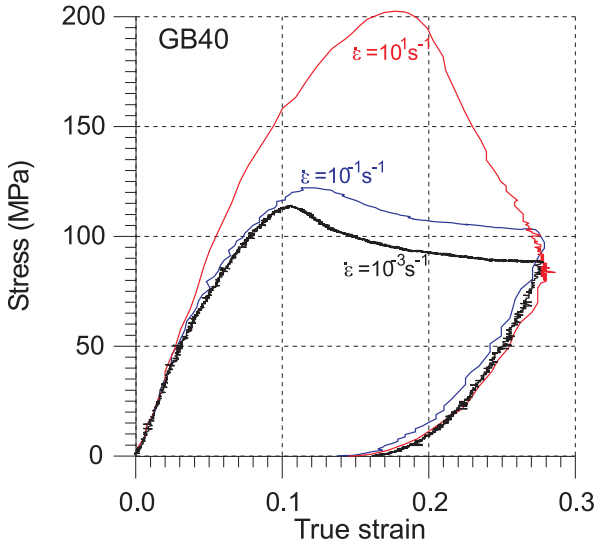

FIG. 5. Stress-strain curves of composite GB40 subjected to uniaxial compression test with various strain rates.

Stress-strain relations obtained during uniaxial compression of GB30 composite for various shear rates are presented in Figs. 4, while those of GB40 composite in Fig. 5. For all the tests, the maximum stress achieved depends on the strain rate; the higher the strain rate, the higher the stress level achieved. This effect is quite significant, i.e. up to 50 % in this range of the strain rates applied. The maximum stresses occur always for the true strain greater than 0.1; the higher the deformation rate, the higher the value of strain at which the maximum stress occurs. Beyond the maximum, a significant decrease in the stress is observed, smooth for the lower deformation rates which was caused by the fiber damage, and rapid in the case of the higher deformation rates, probably caused by coarse cracks of the composite specimens.

The results presented in Figs. 4 and 5 confirm that by using the composite with higher reinforced fibers concentration, usually higher stresses are assured. Namely, for the composite GB40, specified by higher contribution of the reinforced fibers, significantly higher stresses level was achieved.

Furthermore, looking at the photograph of the composite specimen, taken before and after the uniaxial compression test, one can notice that the specimen changed its shape due to the compression and takes an ellipsoidal shape. In order to estimate the changes of the specimen shape for all the tests, the maximal and the minimal axes of its ellipsoidal cross-section were measured. As a measure of the specimen shape evolution, the ratio of maximal to minimal axes has been

calculated. For both kinds of the composite, the obtained values of the ratio were found to be between 0.90 and 0.96. Moreover, a correlation between the maximal compression stresses and the specimen shape evolution was noticed. Higher maximal stresses were achieved in these specimens, the cross-section shape of which was still closer to circular.

3.2. High strain rates

The stress-strain characteristics, obtained for higher strain rates using SHPB technique and calculated on the basis of equations presented in Sec. 2.1, are presented in Figs. 6, 7 and 8. All the curves have been obtained as a result of the first passage (transfer) of the stress pulse through the specimen. Each pulse was followed by a set of the subsequent pulses, which originate as a result of reflection at the ends of the bars and also influenced the specimen deformation. It means that the final state of the composite specimen: the shape, the microstructure, the temperature, etc., is a cumulative result of many pulse stress passages. An example of the stress-strain characteristics, obtained for three GB30 specimens subjected to uniaxial compression test with higher strain rates using SHPB is shown in Fig. 6. The obtained data scatter is reasonable.

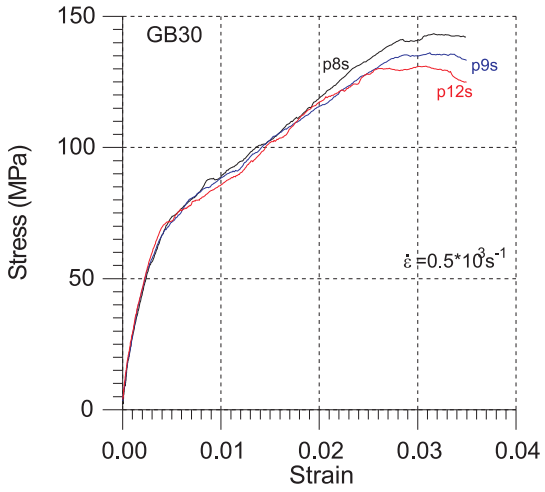

Fig. 6. Stress-strain relations of composite GB30 subjected to dynamic compression tests with long projectile (p8s, p9s, p12s – test numbers).

In order to assure various values of the supplied energy, related to the strain range, three kinds of the projectile were used. The obtained results, namely the stress-strain characteristics, found for various kinds of the applied projectiles are presented in Figs. 7 and 8. The velocity of the projectile, i.e. the pressure of the gas in the gas-gun, has to be chosen high enough in order to evoke a proper

signal in the composite specimen, i.e. which could be registered in the stress-strain characteristics. On the other hand, the stress pulse had not to be too high as not to exceed the elastic limits of the incident and the transmitter bars.

In this approach, three tests for each composite, under three rates of deformation due to various projectile lengths were performed: 0.2×10^3 s^{-1}, 0.35×10^3 s^{-1} and 0.5×10^3 s^{-1}.

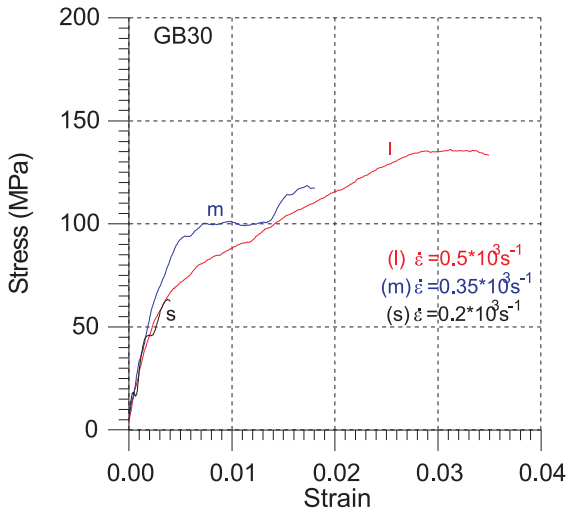

FIG. 7. Stress-strain curves of composite GB30 subjected to dynamic axial compression test with various projectiles length; l, m, s – long, middle, and short projectiles.

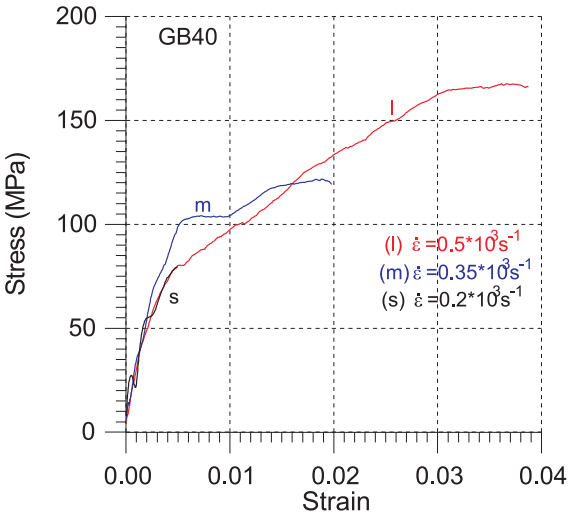

FIG. 8. Stress-strain relations of composite GB40 subjected to dynamic axial compression test with various projectile lengths; l, m, s – long, middle, and short projectiles.

The stress-strain characteristics were calculated using Eqs. (2.6) and (2.7). The plastic deformation of the specimens subjected to dynamic loading in a Hopkinson bar is usually very small; the changes of the composite specimen thickness due to the test do not exceed 0.01–0.02 mm.

The stress-strain curves obtained during the dynamic compression tests do not depend too much on the rate of deformation in the applied range of deformation rate (10^3 s^{-1}). Some observed discrepancies were mainly caused by variation in the mechanical energy supplied by the projectiles with various lengths to the incident bar and then, in form of the wave signals, to the transmitted bar.

Analyzing of the calculated stress-strain curves (Figs. 6, 7 and 8) one can notice that most information can be deduced from the results obtained from the tests carried out with the long projectiles, since due to their high energy, it gives the highest deformation range. The highest energy of the long projectile is accompanied by the highest stress and the strain values.

Two ranges of deformation could be distinguished in the stress-strain curves obtained by the long projectile:

1-st, characterized by a high tangent modulus of $\sigma(\epsilon)$ characteristics.

2-nd, characterized by a significantly smaller tangent modulus of $\sigma(\epsilon)$ curves.

In the second range of the deformation, a rupture of reinforced fibers takes place which causes a higher scatter of the obtained results and significantly affects the stress-strain characteristics.

Looking at the stress-strain curves presented in Figs. 6, 7, 8 one can notice that the mechanical energy supplied to the specimen was probably too small, even in the case of the long projectile (l), in order to obtain the ultimate stress level for this composite. On the other hand, it also means that the composite strength is really high. Nevertheless, the calculated stress values are comparable with the maximum stresses obtained during quasi-static tests for the maximal strain rate $\dot{\epsilon} = 10^1$ s^{-1}. It confirms that the methodology of measurements and final data calculations, applied for the dynamic investigations, is correct.

The energy of the middle projectile (m) was lower than the longer one, so the levels of the stress and the strain obtained were also lower. After the elastic stress limit, a significant influence of fibers rupture on the $\sigma(\epsilon)$ characteristics was observed; Figs. 6 and 7.

For a short projectile (s), the achieved strain did not exceed the elastic range of deformation. The discrepancies between the $\sigma(\epsilon)$ characteristics are caused by a too small length of the projectile in relation to the incident bar diameter, causing non-uniaxial stress waves in the bars.

Generally, it can be concluded that for all the compression tests, higher stresses were achieved for the composites with higher reinforced fibers ratio. During the dynamic compression tests, using the SHPB technique, significantly higher strain range and more reliable results were found using the long projectile.

4. Modeling of the compression test

The stress-strain characteristics obtained for GB30 and GB40 composites subjected to compression test make a basis for the specification of the viscoplasticity model. A polymer matrix of a fibre-reinforced composite can show all the features of a glassy, brittle or an elastic rubber or a viscous liquid, depending on the temperature and the strain rate. The glass-transition range of these variables exists in which the polymer is neither glassy nor rubber-like (cf. WARD [11] for more detailed discussion). In this region, plastic behaviour is observed. According to SELL [12], by plastic deformation we understand the component of the total deformation that is not recovered after the material has been unloaded during the time equivalent to the loading duration. The elementary microscopic mechanisms of inelastic deformation are discussed by ARGON [13]. In general, the dependence of yield limit on strain rate and temperature is observed and theory of viscoplasticity can be applied in such a situation, see for example PERZYNA [14]. The experimental observations performed by transmission optical microscopy and also by scanning electron microscopy reported in SELL *et al.* [15] reveal the activation of crazes and shear bands: *"The crazes are perpendicular to the tensile axis. They are 100 μm long on average and their thickness is too small to be resolved. The shear bands are inclined about 45° on the tensile axis and form a network of lines across the specimen. It is interesting that shear bands seem very often to start and finish near craze tips."* – p. 3865 in SELL *et al.* [15]. This means that the main mechanism of large plastic strains in solid polymers is related to the interplay of shear banding and crazing. On the other hand, the results presented in ZEBARJAD *et al.* [16] devoted to the study of the influence of short fibres and their adhesion to the matrix on the deformation behaviour of polypropylene composites containing 30 wt% of glass fibres with an average length of 6 mm and 13 μm diameter, reveal the both mentioned above mechanisms in the pure polypropylene. They are formed at an angle of about 45° to the direction of the remote loading. Introduction of glass fibres causes the appearance of a large number of crazes, which form perpendicular to the loading direction. As it is stated in ZEBARJAD *et al.* [16], p. 1009: *"Further propagation of the craze needs additional energy to overcome the barrier. The energy provided by further stretching of the samples causes extra crazes forming in the matrix, in the vicinity of the original craze. As seen in Fig. 4b* (cf. ZEBARJAD *et al.* [16], p. 1011), *further loading of the sample causes the new crazes to touch each other and grow in the matrix."* Although it is not clearly stated by the authors in ZEBARJAD *et al.* [16], the pictures made with the use of scanning electron microscope, cf. Fig. 1a and 4b in ZEBARJAD *et al.* [16], show that an additional mechanism of plastic strain contributes to the craze development and thickening. Our hypothesis is that micro-shear bands developing within the polymer matrix are

responsible for the plastic strain. Furthermore, we assume that the mechanisms of micro-shear-banding and crazing on the microscopic level, within the scale of (10÷100) μm, contribute to the mechanism of plastic strain of the composite on the macroscopic level, which can be assumed as an overall shear banding. The corresponding RVE is related with the mean length of the glass fibre.

4.1. Constitutive description of inelastic deformation

The above-mentioned discussion leads to the hypothesis that a multiscale approach, which was proposed in relation to plastic flow of metals accounting for shear banding, in refs. by PĘCHERSKI [17–20], can be extended to describe plastic deformation of polymers and polymer matrix composites. Among many possible realizations of shear banding processes one can single out the group of processes characterizing, at least approximately or for sufficiently long deformation paths, with the same contribution of two systems of shear bands, i.e. $f_{SB}^{(1)} = f_{SB}^{(2)}$, where $f_{SB}^{i}$is the shear banding function describing the contribution of the shear banding system $i = 1$ and $i = 2$, respectively, in the total plastic shear strain rate, PĘCHERSKI and KORBEL [19]. On the other hand, the non-symmetric activation of shear bands can be induced by a sufficiently large change of the loading direction or rotation of the principal axes of the stress tensor in the inhomogeneous deformation process caused by boundary conditions. Therefore, it is postulated in PĘCHERSKI and KORBEL [19] that:

$$\Delta f_{SB} = 0 \quad \text{for} \quad \delta \in [0,\ \delta_c] \quad \text{and} \quad \Delta f_{SB} = A(\delta) \quad \text{for} \quad \delta \in \left(\delta_c,\ \frac{\pi}{2}\right], \tag{4.1}$$

where $\cos\delta = \dfrac{\boldsymbol{\tau}' : \boldsymbol{\mu}_F}{\left|\overset{\circ}{\boldsymbol{\tau}}\right|}$. The function $A(\delta)$ being a measure of the mentioned asymmetry of shear banding, should be identified from numerical simulations of the experiment accounting for the change of loading direction.

Because of the above assumptions, the plastic flow laws take the form:

- For the case in which the loading direction described by the objective rate of stress $\overset{\circ}{\boldsymbol{\tau}}$ is pointing at partially active range, i.e. for $\delta \in \left(\delta_c,\ \dfrac{\pi}{2}\right]$

$$\mathbf{D}^p = \frac{\overset{\circ}{\boldsymbol{\tau}} : \boldsymbol{\mu}_F}{2h(1-f_{SB})}\boldsymbol{\mu}_F + \frac{\overset{\circ}{\boldsymbol{\tau}} : \boldsymbol{\mu}_F}{2h(1-f_{SB})}\frac{A(\delta)\tan 2\beta}{\left\|\overset{\circ}{\boldsymbol{\tau}'}\right\|\sin\delta'}\left[\overset{\circ}{\boldsymbol{\tau}'} - \left(\overset{\circ}{\boldsymbol{\tau}} : \boldsymbol{\mu}_F\right)\boldsymbol{\mu}_F\right], \tag{4.2}$$

- For the case in which the objective rate of stress $\overset{\circ}{\boldsymbol{\tau}}$ is pointing at fully active range, i.e. for $\delta \in [0,\ \delta_c]$:

$$\mathbf{D}^p = \frac{\overset{\circ}{\boldsymbol{\tau}} : \boldsymbol{\mu}_F}{2h(1-f_{SB})}\boldsymbol{\mu}_F\,, \qquad \boldsymbol{\mu}_F = \frac{1}{\sqrt{2}k}\boldsymbol{\tau}'. \tag{4.3}$$

The Huber–Mises yield condition is assumed: $J_2 = k^2$, where $J_2 = \frac{1}{2}\boldsymbol{\tau}' : \boldsymbol{\tau}'$ and the symbol k denotes the yield limit obtained in a shear test. The above-mentioned assumptions leading to the simplified formula (4.3) find confirmation in experimental observations of metallic materials, which show that the spatial pattern of micro-shear bands does not change for loading conditions that deviate within limits from the proportional loading path, i.e. the load increments are confined to a certain cone (fully active range), the angle of which can be determined experimentally, PĘCHERSKI [18, 19]. The specification of these equations and the identification of the shear banding contribution function f_{SB} are discussed in NOWAK and PĘCHERSKI [20]. Further experimental investigations are necessary in order to validate the discussed extension of the constitutive description of viscoplastic deformations over the glass fibre-reinforced composites.

If the dependence on strain rate comes into play, the viscoplasticity flow law can be applied, PERZYNA [14]:

$$\mathbf{D}^p = \dot{\gamma}^{vp}\boldsymbol{\mu}_F\,, \qquad \boldsymbol{\mu}_F = \frac{1}{\sqrt{2}k}\boldsymbol{\tau}', \tag{4.4}$$

where $\dot{\gamma}^{vp}$ is the viscoplastic shear strain rate determined in the following way:

$$\dot{\gamma}^{vp} = \dot{\gamma}_0 \left[\frac{J_2}{(1-f_{SB})\,[A + B(\gamma^{vp})^n]} - 1\right]^{1/D} \tag{4.5}$$

According to the analysis in NOWAK and PĘCHERSKI [20], the shear banding function takes the form which, according to our assumption, is universal for both crystalline and amorphous materials:

$$f_{SB} = \frac{f_{SB_0}}{1 + \exp(a - b\,|\gamma^{vp}|)}. \tag{4.6}$$

This assumption finds at least partial confirmation in our modelling of experimental results. However, it should be verified in an independent identification test, cf. NOWAK and PĘCHERSKI [20].

The yield condition $J_2 = k_d$ is obtained by inverting (4.5)

$$k_d = (1-f_{SB})\,[A^* + B^*(\gamma^{vp})^n]\left[1 + \left(\frac{\dot{\gamma}^{vp}}{\dot{\gamma}_0}\right)^D\right]. \tag{4.7}$$

For compression test $\sigma_{Yd} = \sqrt{3}k_d$, $\varepsilon^{vp} = \frac{\sqrt{3}}{3}\gamma^{vp}$ and (4.7) reads:

$$\sigma_{Yd} = (1-f_{SB})\;\;[A + B(\varepsilon^{vp})^n]\;\;\left[1 + \left(\frac{\dot{\varepsilon}^{vp}}{\dot{\varepsilon}_0}\right)^D\right], \tag{4.8}$$

where $A = \sqrt{3}A^*$, $B = \sqrt{3}B^*$ and ε^{vp} is the viscoplastic strain and $\dot{\varepsilon}^{vp}$ denotes viscoplastic strain rate.

4.2. Identification of the model

The basic idea of the identification procedure was to determine all material constants without the use of numerical simulations. This was found possible using a direct curve fit to the experimental data, assuming proportional straining and constant strain-rate and temperature. The method of least squares requires the residual sum between the experimental observations and model results to be minimised. This implies that the proposed model of rate-dependent plasticity can be completely calibrated by minimising the residual:

$$F(x) = \sum_{\alpha=1}^{N_\alpha} \sum_{\delta=1}^{N_\delta} \left\{ \sigma_{eq}^{\exp}\left(\varepsilon_\alpha^{vp}, \dot{\varepsilon}_\delta^{vp}\right) - \sigma_{eq}^{\mathrm{cal}}\left(\varepsilon_\alpha^{vp}, \dot{\varepsilon}_\delta^{vp}\right) \right\}^2 , \tag{4.9}$$

where $F(x)$ refers to the residual of the constitutive model with $x = (a, b, f_{SB_0}, A, B, n, \dot{\varepsilon}_0^p, D)$ material constants to be determined. Furthermore, ε_α^{vp} are discrete values of the strains ε_α^{vp}. The symbols $\sigma_{eq}^{\exp}$ and $\sigma_{eq}^{\mathrm{cal}}$ denote the experimental and calculated stresses for the same strain level α, N_α is the number of stress-strain data for the test δ with given strain rate at room temperature, and N_δ is the number of the tests considered. For our constitutive equation Eq. (4.8) we have

$$\sigma_{eq}^{\mathrm{cal}} = \left(1 - \frac{f_{SB_0}}{1 + \exp(a - b\varepsilon_\alpha^{vp})}\right) (A + B(\varepsilon_\alpha^{vp})^n) \left(1 + \left(\frac{\dot{\varepsilon}_\delta^{vp}}{\dot{\varepsilon}_0^{vp}}\right)^D\right). \tag{4.10}$$

The objective function $F(x)$ requires the minimisation subject to determining the value of each constant within a region defined by the lower and upper bounds, that is, for all the material constants.

The domains of the material constants can be determined from their physical significance. For example, according to plastic deformation mechanisms the value of the exponent D should be within the range 0 to 1. Otherwise, the physical significance would be lost. For some constants, e.g. n, it is difficult to determine their limits, although they cannot be negative without losing physical meaning. In this case, a relatively large variation range can be given, so that the optimum points are expected to be included within the region. The domains of the material constants determined from their physical significance for optimisation are given in Table 1.

Table 1. Domains of the material constants.

	GB30, GB40
a	0.0 – 20.0
b	0.0 – 100.0
f_{SBo}	0.0 – 1.0
A [MPa]	0.0 – 20.0
B [MPa]	10.0 – 800.0
n	0.00001 – 3.0
D	0.0 – 1.0
$\dot{\varepsilon}_0^{vp}$ [s^{-1}]	10^{-10} – 10^{-3}

Table 2. Identified material constants for GB30 (Fig. 9) and GB40 (Fig. 10).

	a	b	f_{SB_0}	A [MPa]	B [MPa]	n	D	$\dot{\varepsilon}_0^{vp}$ [s^{-1}]
GB30	1.20	17.9	0.9	8	650	1.15	0.08	10^{-9}
GB40	1.05	19.5	0.9	8	600	1.02	0.08	10^{-9}

The constants determined using best curve fitting optimisation technique were used to plot the theoretical curves, which are compared with the experimental results shown in Figs. 9 and Fig. 10.

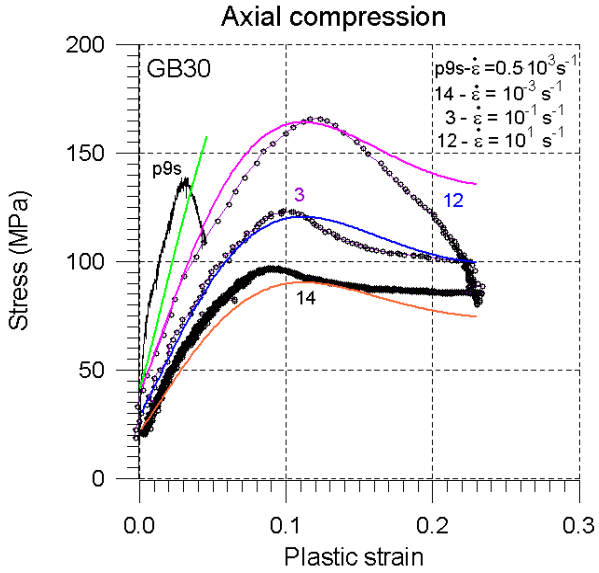

FIG. 9. Comparison of theoretical predictions with the stress-strain curves obtained during axial compression of GB30 composite with three strain rates. The curves labelled 3, 12, 14 were taken from experiments; (Figs. 3, 4). The curves calculated theoretically are plotted using thin smooth lines.

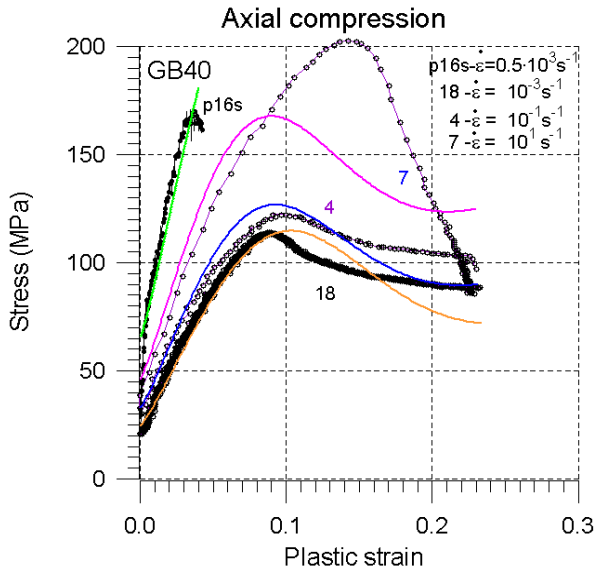

Fig. 10. Comparison of theoretical predictions with stress-strain curves obtained during axial compression of GB30 composite with three strain rates. The curves labelled 4, 7, 18 were taken from experiment; (Fig. 5). The curves calculated theoretically are plotted using thin smooth lines.

The results displayed in the figures show quite good correlation of the viscoplastic model accounting for shear banding with experimental data within the wide spectrum of strain rates. The discrepancy between the results of theoretical prediction and experiment shown in Fig. 10, curve 7, is probably produced by the effect of non-uniform distribution of the glass fibers in the material from which the specimen was cut out. Additional tests are necessary to obtain the repeatable results, which could validate the theoretical prediction.

5. Conclusion

Static and dynamic uniaxial compression tests for two types of glass fibre-reinforced polypropylene composites were presented. The obtained results confirm high mechanical properties of the composite within a wide spectrum of the strain rates. Moreover, the stress-strain curves manifest significant influence of the strain rate on the composite mechanical behaviour, even in the quasi-static range of deformation. The maximal stresses achieved depend on the strain rate; the higher the strain rate, the higher the stress level. This effect was quite significant, up to 50% in the applied range of the strain rates.

The maximal stresses obtained both during quasi-static and dynamic compression tests are higher for the composite with a higher reinforced fibers fraction.

The higher the ratio of the reinforcing fibers, the higher the material strength was achieved. However, the differences are not so significant and probably they are also caused by the ordinary measurement data scatter.

The maximal stresses have always occurred for the true strains higher than 0.1; the higher the deformation rate, the higher the value of the strain where the maximal stresses were found. Beyond the maximum, a significant decrease of the stress was observed, smooth for lower deformation rates which was caused by the fiber damage, and rapid in the case of higher deformation rates, probably also caused by the specimens coarse cracks.

The obtained stress-strain curves show quite good repeatability in relation to such kind of composites, especially in the elastic range of deformation. Beyond the elastic limit, a discrepancy between the curves of the particular specimen has been observed which was probably related to the reinforcing fibers fracture. Some discrepancies between the curves indicate a non-uniform distribution of the density and orientation of the composite fibers.

A correlation between the maximal stresses and the shape change of the round flat specimens caused by the compression process has been observed. Higher maximal stresses were recorded for the specimens, the cross-sectional shape of which after the compression test remained closest to circular one.

During the dynamic compression tests, using the SHPB technique, significantly higher strain range and more reliable results were found using the long projectile, while for the middle projectile the stress and the strain values were much smaller, and for the short projectile the achieved maximal strains did not exceed the elastic strain range.

Two deformation stages can be distinguished in the calculated stress-strain curves for the dynamic testing: elastic and non-elastic – related to the fiber rupture, similarly to that found during quasi-static tests. The plastic deformation of the specimens subjected to dynamic deformation is very small. It can be concluded both on the basis of the stress-strain characteristics as well as on the basis of almost insignificant specimens shape changes.

A viscoplasticity model of the material behavior during the deformation has been developed and the material constitutive parameters have been calculated. Specification of the parameters and description of the methods used for their identification have been worked out on the basis of the stress-strain characteristics obtained for GB30 and GB40 composites subjected to compression. The results were discussed in terms of the deformation processes and the material non-homogeneity.

The experimental investigations revealed a certain anisotropy, which could be classified as orthotropic or transversal. In such a case the concept of elastic proper states and the energy-based approach to yield criteria for anisotropic solids proposed by J. RYCHLEWSKI [21, 22] and studied further, e.g.,

in Kowalczyk *et al.* [23, 24] can be applied for the formulation of appropriate model of elasto-viscoplasticity of glass fibre-reinforced polymers. Further studies are necessary to identify the anisotropy of elastic properties and yield limit of such composites.

Acknowledgment

This research has been carried out with the financial support of the Polish Ministry of Science under Grants No. 8TO7A04620, 4T08A06024, EUREKA E! 3064, and the Japan Society for Promotion of Sciences – Post-doc ID No. P04774 and Joint Research on Scientific Collaboration: No. 6612. The authors also wish to extend their thanks to L. Urbanski (IFTR PAS) for technical advice.

References

1. T.E. Tay, H.G. Ang, V.P.W. Shim, *An empirical strain rate-dependent constitutive relationship for glass-fibre reinforced epoxy and pure epoxy*, Compos. Struct., **33**, 4, 201–210, 1995.
2. J.J. Horst, N.V. Salienko, J.L. Spoormaker, *Fibre-matrix debonding stress analysis for short fibre-reinforced materials with matrix plasticity, finite element modelling and experimental verification*, Compos. Part A-Appl., S **29**, 5–6, 525–531, 1998.
3. J. Fitoussi, G. Guo, D. Baptiste, *A statistical micromechanical model of anisotropic damage for SMC composites*, Compos. Sci. Technol., **58**, 5, 759–763, 1998.
4. M. Pinfold, G. Calvert, C. Garroch *et al.*, *A comparison of thermoelastic and numerical stress results for moulded composites plates*, Key Eng. Mat., **144**, 117–125, 1998.
5. P.P. Camanho, F.L. Matthews, *A progressive damage model for mechanically fastened joints in composite laminates*, J. Compos. Mater., **33**, 24, 2248–2280, 1999.
6. M. Piry, W. Michaeli, *Stiffness and failure analysis of SMC components considering the anisotropic material properties*, Macromol. Mater. Eng., **284**, 11–12, 40–45, 2000.
7. F. Ellyin, Z.H. Xia, *Rate-dependent constitutive modelling and micro-mechanical analysis of fibre-reinforced metal-matrix composites*, J. Mech. Phys. Solids., **49**, 11, 2543–2555, 2001.
8. J.R. Klepaczko, *Lateral inertia effects in the compression impact experiment*, IFTR Reports 17, Warsaw 1969.
9. J.A. Zukas, T. Nicholas *et al.*, *Impact Dynamics*, John Wiley and Son, 1982.
10. U.S. Lindholm, J. Mech. Phys. Solids, **12**, 317, 1964.
11. I.M. Ward, *Mechanical Properties of Solid Polymers*, Wiley, London 1971.
12. C.G. Sell, *Plastic deformation of glassy polymers: Constitutive equations and macromolecular mechanisms*, [in:] Strength of Metals and Alloys, H.J. McQueen *et al.* [Eds.], 1943–1982, Pergamon Press, Oxford 1986.

13. A.S. ARGON, *Rate processes in plastic deformation of crystalline and noncrystalline solids, 175-230, in: Mechanics and Materials: Fundamentals and Linkages*, M. C. MEYERS *et al.* [Eds.], J. Wiley, New York 1999.

14. PERZYNA, *Fundamental problems in viscoplasticity*, Advances in Mechanics, **9**, 243–377, 1966.

15. C.G. SELL, J.M. HIVER, A. DAHOUN, *Experimental characterization of deformation damage in solid polymers under tension, and its interrelation with necking*, Int. J. Solids Struct., **39**, 3857–3872, 2002.

16. S.M. ZEBARJAD, A. LAZZERI, R. BAGHERI, S.M. SEYED REIHANI, *Role of the interface on the deformation mechanism of glass fiber/polypropylene composites*, J. Mat. Sci. Letters, **21**, 1007–1011, 2002.

17. R.B. PĘCHERSKI, *Macroscopic measure of the rate of deformation produced by micro-shear banding*, Arch. Mech., **49**, 385–401, 1997.

18. R.B. PĘCHERSKI, *Macroscopic effects of micro-shear banding in plasticity of metals*, Acta Mechanica, **131**, 203–224, 1998.

19. R.B. PĘCHERSKI, K. KORBEL, *Plastic strain in metals by shear banding. I. Constitutive description for simulation of metal shaping operations*, Arch. Mech., **54**, 603–620, 2002.

20. Z. NOWAK, R.B. PĘCHERSKI, *Plastic strain in metals by shear banding. II. Numerical identification and verification of plastic flow law accounting for shear banding*, Arch. Mech., **54**, 621–634, 2002.

21. J. RYCHLEWSKI, *Elastic energy decomposition and limit criteria* [in Russian], Uspekhi Mekh.-Advances in Mech., **7**, 51–80, 1984.

22. J. RYCHLEWSKI, *Unconventional approach to linear elasticity*, Arch. Mech., **47**, 149–171, 1995.

23. K. KOWALCZYK, J. OSTROWSKA-MACIEJEWSKA, *Energy-based limit conditions for transversally isotropic solids*, Arch. Mech., **54**, 5–6, 497–523, 2002.

24. K. KOWALCZYK, J. OSTROWSKA-MACIEJEWSKA, R.B. PĘCHERSKI, *An energy-based yield criterion for solids of cubic elasticity and orthotropic limit state*, Arch. Mech., **55**, 5–6, 2003.

Received July 23, 2004; revised version April 11, 2006.